Materials Horizons

# Homogeneous Gelation Leads to Nanowire Forests in the Transition Between Electrospray and Electrospinning



| | |
|---|---|
| Journal: | *Materials Horizons* |
| Manuscript ID | MH-COM-05-2020-000872.R1 |
| Article Type: | Communication |
| Date Submitted by the Author: | 15-Jul-2020 |
| Complete List of Authors: | Lei, Lin; Rutgers The State University of New Jersey, Mechanical and Aerospace Engineering<br>Chen, Shensheng; Binghamton University, Department of Mechanical Engineering<br>Nachtigal, Catherine; Rutgers The State University of New Jersey, Mechanical and Aerospace Engineering<br>Moy, Tyler ; Binghamton University, Department of Mechanical Engineering<br>Yong, Xin; Binghamton University, State University of New York, Department of Mechanical Engineering<br>Singer, Jonathan P.; Rutgers, The State University of New Jersey, Mechanical and Aerospace Engineering |
| | |

# Homogeneous Gelation Leads to Nanowire Forests in the Transition Between Electrospray and Electrospinning

Lin Lei[1], Shensheng Chen[2], Catherine J. Nachtigal[1], Tyler F. Moy[2], Xin Yong[2], Jonathan P. Singer[1]*

[1]Rutgers University, Department of Mechanical and Aerospace Engineering, Piscataway, NJ, USA.

[2]Binghamton University, Department of Mechanical Engineering, Binghamton, NY, USA.

*Correspondence to: jonathan.singer@rutgers.edu

## New Concepts

This manuscript introduces a means to create polymer nanowire forests and foams on a wide variety of surfaces by manipulating the rheology of electrostatically-sprayed droplets. It also answers the question of why such forests have not been observed previously, despite over a century of electrostatic spray research and decades of their industrial ubiquity. At the transition between electrospray nanoparticles and electrospun nanowire mats—where the forests would reside—the atomized droplets rapidly evaporate as they travel to their target, leading to the formation of an immobile shell that creates bead-on-string morphologies. If the droplets could evaporate homogeneously, however, the increase in viscosity would allow each droplet to electrospin into its own wire, composing a forest or foam. We demonstrate this phenomenon both through electrostatic dissipative particle dynamics modeling and in a physical system of methylcellulose. Methylcellulose and another cellulose ether, hydroxypropyl methylcellulose, are the only materials demonstrated thus far to naturally form these morphologies. These cellulose ethers have recently been revealed to exhibit a unique fibrillar gelation in flow that may explain why they can solidify uniformly during the sub-second electrospray flight, which usually requires minutes to hours.

COMMUNICATION

# Homogeneous Gelation Leads to Nanowire Forests in the Transition Between Electrospray and Electrospinning

Received 00th January 20xx,
Accepted 00th January 20xx

DOI: 10.1039/x0xx00000x

Lin Lei,[a] Shensheng Chen,[b] Catherine J. Nachtigal,[a] Tyler F. Moy,[b] Xin Yong[b] and Jonathan P. Singer[a]*

**The morphology of coatings created by electrostatic deposition can be generally divided into three categories: wire mats, particles, and films. At intermediate regimes, there should exist nanowire forests as a mixture of wire and particulate deposition, but these have yet to be observed as a dominant morphology. We utilized electrostatic dissipative particle dynamics simulations to reveal that the barrier to forming nanowire forests is the directional nature of evaporation, implying that they should form were evaporation homogeneous. Experimentally, we utilized electrospray deposition (ESD) to explore the spray of a fibril gel former, methylcellulose (MC) in water:ethanol mixtures. MC possesses a lower critical solution temperature (LCST) in water and water:ethanol blends. Above the LCST, MC and water phase separate concurrently with the rapid evaporation of ethanol, forming a shear-thickening, homogeneous gel phase. In the ESD process, the strongly entangled polymer solution as a result of gelation electrospins on a drop-by-drop basis to create forests of individual nanowires. To verify this mechanism, we employed different viscosities of MC by ESD through changes in spray temperatures, molecular weight, loading concentration, flow rates, spray distances, and additive content. The results reveal that lowering the viscosity of the gel increases the aspect ratio of formed nanowires. Similarly, the incorporation of additives that lead to too high or too low a viscosity prevents the formation of nanowires in ESD. Our study indicates that the homogenous evolution of viscosity is necessary for nanowire forest formation and that the specific viscosity further controls the morphology of the forests.**

## Introduction

There are several distinct communities in the field of electrostatic deposition. Electrostatic corona spray has been a standard tool for automotive, pharmaceutical, agricultural, and other commercial paint applications. Filament-based approaches in the far field (i.e. electrospinning) have recently attained industrial applications for making nanofiber mats as filters and scaffolds,[1] while the near field methods (i.e. electrohydrodynamic printing) enables direct writing of polymer or nanostructured filaments. Electrospray, despite being the first method developed in electrostatic deposition,[2] has been primarily employed in metrology through mass ionization.[3] Recently, however, electrospray deposition (ESD) has gained increasing attention in nanotechnology and biomedical applications with its unique ability to deliver nanograms of material per droplet. ESD has been utilized for, among other applications, nanostructured polymer coatings, the delivery of cells and other bioactive media, and the synthesis of hierarchical functional oxides.[4, 5] Even being restricted to dissolved solutions (e.g. polymer or other small molecule processing), the electrostatic deposition exhibits a breakdown of deposit morphologies into "wires",[6-9] "particles",[6, 7, 9-16] and "films",[17] with the wires (produced by filament-based approaches) lying flat on a substrate, the particles (produced by electrostatic corona spray or ESD) forming hierarchical coatings, and the films, which can arise from any of the methods, covering the entire target region or dewetting into localized regions. A brief collection of examples, with a few lesser-observed morphologies, can be found in Table S1.

The deciding factor in the formation of these morphologies is the competition between the instantaneous viscosity of the solution and the surface forces during the process. In polymeric solutions, this viscosity is determined by the entanglement and relaxation of the chains,[18] but it can also be achieved by other mechanisms, such as hydrogen bonding in sugar solutions.[19] If the viscous forces dominate, droplets do not form and instead the solution spins as a filament. With the whipping of the electrostatic spinning process, this regime produces mats of in-plane nanowires (NWs). If the entanglement only occurs during solvent evaporation, a particulate spray is formed. If the

[a] Rutgers University, Department of Mechanical and Aerospace Engineering, Piscataway, NJ, USA.
[b] Binghamton University, Department of Mechanical Engineering, Binghamton, NY, USA.

†Electronic Supplementary Information (ESI) available: See DOI: 10.1039/x0xx00000x

viscosity does not appreciably increase during the deposition process, a film is formed in a wetting regime. Intermediate regimes of processing lead to other desirable (or undesirable) effects. For example, a certain degree of film-forming tendency in wire or particulate sprays can lead to solvent-welding of the mats or particles into bicontinuous films. This is advantageous for improving the mechanical robustness of the deposits and promoting resistance to the corona pitting, which is a notable failure mode of powder electrostatic sprays.[20] Despite this, one surprising observation is that there are no reports of ESD of NW forests or foams, which should be a natural intermediate regime between wire and particulate depositions. The forest morphology is characterized by preferential alignment of short NWs along the direction of the field, while the foam morphology is a multilayer of such forests that maintain some degree of alignment. These morphologies can be interpreted as an intermediate of particulate and NW mat morphologies, since the filamentation will naturally occur in the direction of the driving force. This is analogous to the near-field electrohydrodynamic printing, where the high field pulls an electrospun filament directly to the substrate before the far-field whipping that creates mats initiates.[21] All that should be necessary for this to occur is for the instantaneous viscosity of a sprayed droplet in ESD to become great enough when the droplet approaches the substrate so that each droplet presents a similar phenomenological arrangement of the printing nozzle.

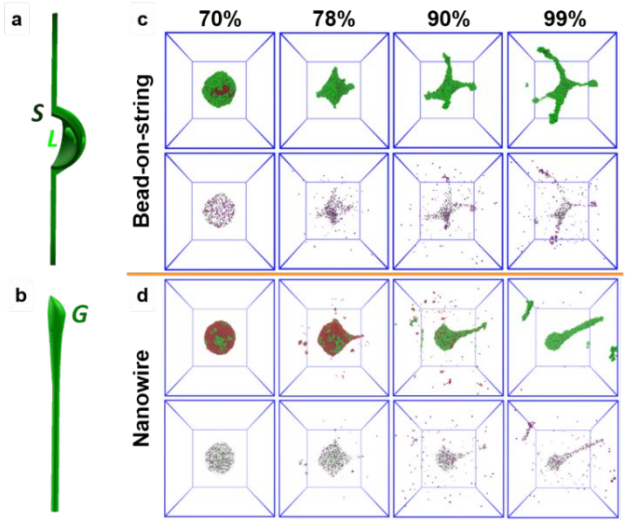


**Fig. 1** Formation of bead-on-string and nanowire morphologies in electrospray deposition. (a) Schematic of the proposed bead-on-string formation mechanism where the immobile solid-like ("S", dark green) exterior of the droplet is unable to participate in the fission, while the more-liquid interior ("L", light-green) is able to escape to the surface to participate in fission. (b) Schematic of the formation of a nanowire where the intermediate viscosity gel ("G", green) is extruded into an asymmetric filament. (c,d) Dynamic evolution of droplet morphology and ion distribution in the DPD simulations under the (c) physical evaporation (100 beads per time step) and (d) homogeneous removal of solvent bead (2 beads per time step), which shows the development of the bead-on-string and nanowire geometries respectively. The number denoting each column is the percentage of removed solvent beads, representing different times in the electrospray transit. The green and red spheres in the upper panel are polymer and solvent beads. The magenta spheres in the bottom panel are charged ion beads while the light green dots in the background represents both polymer and solvent. Vapor beads are not displayed for clarity.

Certainly, the viscosity of evaporating droplets increases during ESD and there exist transition behaviours. The most common and intriguing observation in our studies at the transition between ESD and electrospinning is a "bead-on-string" geometry (Fig. 1a), which has previously been applied in electrospinning as a means to decorate the mats for wetting manipulation.[22-24] In the "bead-on-string" mechanism, the poles (and occasionally multiple other portions[16]) of the electrostatically deformed droplet will each produce a filament, while leaving some intact central mass. These filaments are a natural evolution of the Coulomb fission process, where an ESD droplet, upon reaching the Rayleigh limit of surface charge under rapid solvent evaporation, will create additional child droplets through the creation of Taylor cone pseudopods.[25-27] As classified by Almería et al.,[16] should Coulomb fission occur in a more viscous (*i.e.*, entangled) droplet, filaments are generated instead of solvent offsprings being ejected with no polymer mass contained. Because of the directional nature of evaporation, the exterior of the droplet will form a less-mobile skin, while the interior of the droplet will be the most fluid, so it has the ability to migrate to the poles. As a result, the formation of filaments never employs the entirety of a droplet: droplets either produce other droplets and then solidify or produce filaments. This can also be viewed via the electrostatic capillary number of the droplet during evaporation. If the evaporation halts when the Ca is high for the whole droplet, there will likely be particles or shells as the final morphology. Alternatively, if the Ca is low for the interior of the droplet, but high for the shell, a bead-on-string morphology will form. This behaviour has been previously observed by Merrill et al., labelled as "comet" particle.[28] In this report, they also observed some elongated particles, but were only a small fraction of the population. Zhao et al. also reported some population of "nanopillars" at specific spray distances in photovoltaic polymers that show shear-oriented crystallinity.[29] Almería et al. also demonstrated that some population of tailed and elongated particles of aspect ratio (AR) <4 could be obtained in poly(lactide-co-glycolide) polymer solutions by the deliberate selection of polymer loading (and thereby entanglement concentration on fission) within a range of 3~7 vol%.[16]

The limited number of these results arises from the need for independent control of the instantaneous viscosity and evaporation. What would be required to reliably produce a NW forest is a rapid increase in viscosity of the entire droplet near a fission event (Fig. 1b). This is an atypical behaviour for an in-flight droplet evaporating under substantial forced convection. Further, this increase has to occur in the timescale of a typical electrospray transit, which is $O$(100 ms). This is uncharacteristically fast for a majority of kinetic processes in solution that often progress by nucleation or diffusive processes. One transformation that could potentially satisfy these requirements is the homogenous formation of a gel.

To test this hypothesis, we approached the problem using coarse-grained computational modelling of a model system and methylcellulose (MC) ESD experiments. The goal of the simulations was to establish that if homogenous viscosity transitions did occur, they would be associated with the

tendency to form singular NWs, while heterogenous viscosity transitions would lead to shells, particles, or beads-on-strings. The experiments then established that the ESD of MC solutions in water:ethanol mixtures could satisfy the required kinetics due to the specific gelation mechanism of these materials.

## Results and Discussion

**Simulation Results and Discussion**

We conducted electrostatic dissipative particle dynamics (DPD) simulations[30-35] to uncover the morphology evolution of electrified droplets in flight governed by the interplay between electrohydrodynamics and evaporation. The model system was a charged droplet containing 10% polymer chain beads and 90% solvent beads with charge beads distributed evenly in both phases. Evaporation was modelled by removing solvent beads locally at the droplet surface. The rate of evaporation can be controlled by the number of beads removed per time step. This approach mimics the physical mass transport at the liquid-vapor interface and reproduces the $D^2$ law as shown in Fig. S1.[36] The initial charge density of the droplet was small so that a stable spherical droplet could be obtained. Upon solvent evaporation, the charge density increases and eventually drives the deformation and fission of the droplet.

Fig. 1c shows the representative morphologies of a polymeric droplet during a Coulomb fission event. As the charge density reached the Rayleigh limit, multiple Taylor cone pseudopods were formed at the surface of droplet (Supplementary Movie 1). Ion beads were emitted from the pseudopods into the vapor phase, followed by the protrusion of polymer chains from the central mass. Due to the strong entanglement of polymer chains, the capillary rupture of the filaments was inhibited. Instead the central region of the filaments underwent a necking process while the tips formed bulges. These orchestrated events lead to the bead-on-string morphology. The polymer density characterization confirms the evaporation-driven skin formation (Fig. S2a).

The desired gelation of a polymer network rapidly and uniformly increases the droplet viscosity. To model this regime of ESD, we performed another set of simulations by removing randomly selected solvent beads from the droplet, not limited to the surface. This approach guarantees a homogeneous distribution of polymer in the entire droplet during the morphology development. Fig. 1d demonstrates that the multiple protrusions of polymer filaments under Coulomb fission were strongly suppressed. Only one filament was observed in the simulation, resulting in a tadpole-shaped droplet (Supplementary Movie 2). As this filament further elongated and grew, a nanowire was formed eventually. Additional simulations at different rates of removing the solvent beads shown in Fig. S3 indicates the morphology development is determined by droplet viscosity distribution and not sensitive to other simulation conditions. The transition from the bead-on-string to nanowire morphologies was observed under highly suppressed evaporation, where polymer density remains uniform (Fig. S2b, c).

**Electrospray Results and Discussion**

MC possesses a lower critical solution temperature (LCST) in water and water:ethanol blends, though ethanol is predicted to rapidly evaporate. Above the LCST, the MC and water gel and also phase-separate. The mechanisms for the gelation in particular have been an active topic of research. Recent work, much of it conducted by Bates and Lodge, suggests that the formation of MC gels is mediated by fibrils that form from aggregates that assemble in the low temperature solution.[37-39] Also relevant to the ESD process is that, once formed, the fibril network is shear thickening due to high chain rigidity[40] and is also highly viscous in extension.[41] Prior kinetic investigations have shown three characteristic time scales for MC gelation,[42] with the most rapid potentially satisfying the required kinetics.

MC solutions were sprayed at room temperature to ensure they are homogeneous liquid mixtures. Initially, it was expected that the spray target would need to be above the LCST (~40 °C at 1%) to obtain the gelation and NW formation, and Fig. 2 shows characteristic SEM images from MC conducted at different substrate temperatures, flow rates, and distances. At room temperature, there is a greater tendency to form agglomerated structures; however, the NW formation is remarkably robust at all temperatures. This is notable because we were unable to obtain NWs in poly(N-isopropylacrylamide) (PNIPAAm, Fig. S4a), another LCST, but non-gelling polymer, even at high temperature that may be expected to trigger a spinodal phase separation. The same was true of gelatin that forms strong gels through a different, upper critical solution temperature (UCST), formation mechanism (Fig. S4b), which only showed electrospinning and bead-on-string morphologies in all conditions tested. NWs were obtained in hydroxypropyl methylcellulose (HPMC), another LCST cellulose ether that forms weak gels (Fig. S4c). It is therefore likely that both the gelation and the fibrillation mechanism that distinguishes cellulose ethers from other polymers is the origin of this difference, which explains why to date NW morphologies have not been extensively reported.

Despite this apparent explanation, the thermodynamic studies of fibrillation have shown this mechanism to require timescales of hours.[37] Were fibril gel formation the critical process, there must be some unique attributes of ESD that accelerate the gel formation. The ESD process is highly non-equilibrium and possesses three distinct characteristics: evaporation, extreme shear/extension rate, and high surface charge. Evaporation will increase the concentration of the sprayed solution; however, were this the key effect, bead-on-string morphologies should be observed as with other evaporation-dominated results. Ionic effects are known to have a large influence on the gelation of polymers, for example, the addition of salts to either lower or raise the LCST of MC.[44] pH is also known to have an effect on gelation kinetics.[45] It is reasonable, therefore, to expect that free surface charge may also alter the gelation behaviour and kinetics. MC gels are also shear thickening.[40] Gomez and Tang verified through high-speed photography that a fission event occurs in <1 $\mu$s. Considering typical droplet sizes in ESD, the magnitude of the strain rate of Coulomb fission can be estimated conservatively at $\dot{\gamma} = 10^6 \sim 10^7\ s^{-1}$. This significant deformation rate may

induce order in the nematic-like fibrils. Certainly, both of these effects, charge and strain, are also at play in electrospinning. Cellulose ethers, primarily HPMC, have been deposited by electrospinning previously; however reports of MC electrospun mats are limited and indicate that the mats are unusually fused[46] in a very similar fashion to the room temperature results reported here. This suggests that the shear/charge-free state of the filaments on the substrate after deposition are more fluid-like, indicating that the gelation is indeed present during the spinning, but relaxes on the substrate. While these are only speculative indications of fibrillation as the likely mechanism, the fact remains that MC and HPMC can form NWs, which, according to the simulation results, indicates a transition in viscosity and the establishment of extensive chain entanglements at a more rapid rate than solvent evaporation.

We now evaluate how modifications in the electrospray parameters can be used to alter or disrupt the morphology of the NWs. It is expected that this behaviour should be very sensitive to changes in the material viscosity and surface charge, and we approached this through changes in (1) flow rate, (2) molecular weight, (3) concentration, (4) spray distance, and (5) additive content. Effects were determined by examining short-time sprays of isolated single wires (Fig. S5-11). Extracted parameters are shown in Fig. 3, with a notional AR defined as the ratio of the mean length and mean diameter of the NWs. While this definition captures some behaviours, it is sensitive to the production of child droplets, that have an oversized effect in reducing the AR considering their low mass fraction of the sprayed polymer.

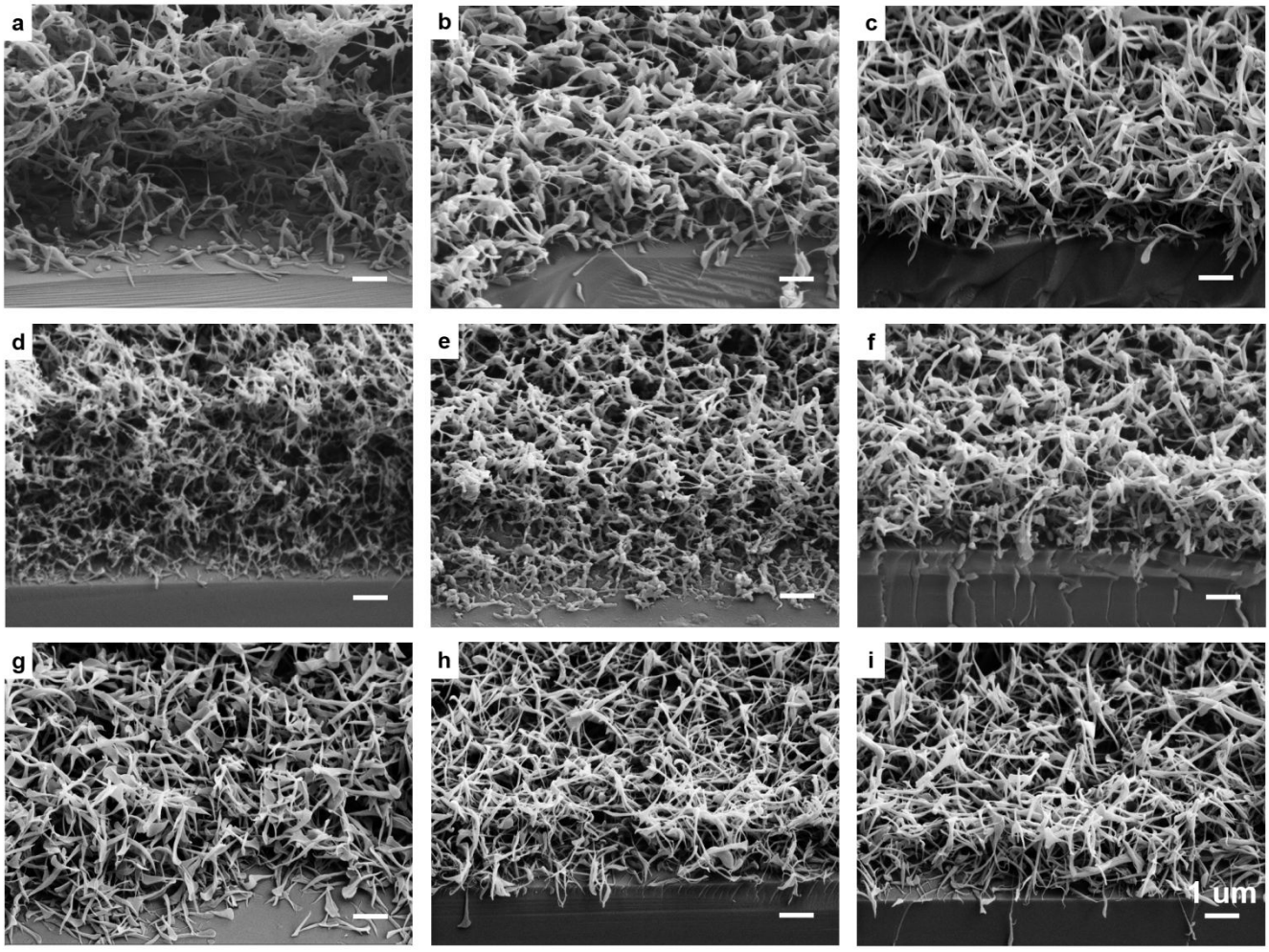


**Fig. 2** Parametric spray of MC nanowires. SEM images of 1 wt%, 14 kDa MC in 3:2 weight-basis water:ethanol blend sprayed with different substrate temperatures, different flow rates and different spray distances. (a) 30 °C, (b) 50 °C, (c) 90 °C at 0.25 mL/hr for 30 min at the spray distance of 4 cm; (d) 0.02 mL/hr, (e) 0.05 mL/hr, (f) 0.15 mL/hr, with a substrate temperature at 90 °C at a constant solids quantity of 1.25 mg and a spray distance of 4 cm; (g) 3 cm, (h) 5 cm, (i) 7 cm, with the flow rate of 0.25 mL/hr and the substrate temperature of 90 °C for 30 min.

Altering the flow rate most directly affects the size of the spray droplets. The flow rate in ESD is known to alter the droplet size proportionally to $Q^{\frac{2}{3}}$ and the droplet charge per volume proportionally to $Q^{-\frac{1}{4}}$,[47] where $Q$ is the flow rate. From the morphologies in Fig. 2, the reduction of diameter of the NWs is readily visible, creating a more open foam-like structure. From the individual wire measurements, the reduction in both length and diameter with reducing flow rate is apparent. If we extrapolate these dimensions into the equivalent sphere diameter, a power law of 0.48 is extracted (Fig. S12), approaching the expected proportionality. At higher flow rates, the aspect ratio and mean wire dimensions appear to stabilize

below the peak value at 0.1 mL/hr. This decrease may be attributed to the increased incidences of child droplets from the slowed evaporation of larger droplets. Larger droplet sprayed at higher flow rates are able to emit child droplets from the forming filament for a longer period of their evolution. At the lowest flow rate of 0.02 mL/hr, mean AR is also greatly reduced despite many of NWs possessing similar ARs to the higher flow rates again because of the production of child droplets. This can be seen directly in the high asymmetry of the 0.02 mL/hr box plot in Fig. 3.

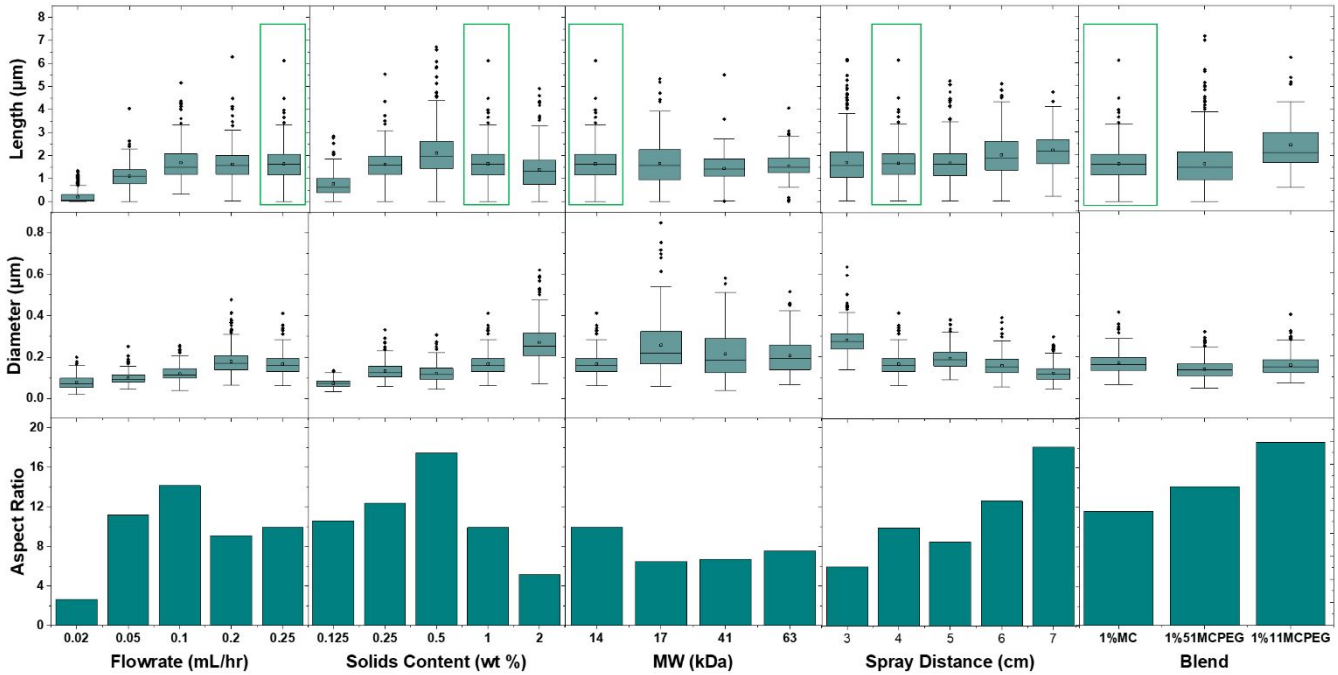


**Fig. 3** Parametric study of nanowire parameters from short-time sprays. Dependence of length (top), diameter (middle), and AR (bottom) of single wires on ESD parameters of MC films at different flow rates (left), solids content (left-middle), MW (middle), spray distance (right-middle), and blending at 5:1 and 1:1 ratio of MC:PEG 400 (right). All sprays were conducted at a substrate temperature of 90 °C from a 3:2 weight-basis water:ethanol blend. The green-boxed sample is the baseline for all sets (1 wt%, 14 kDa MC, 0.25 mL/hr, 4 cm spray distance).

Changes to the concentration, MW, spray distance, and composition at constant droplet size (*i.e.*, flow rate) are expected to affect the dynamic evolution of the droplet viscosity. Increasing the loading of solids or MW notably increases the initial viscosity of sprayed droplets and can be viewed as setting a timer on the NW formation process. When the loading is high, droplets will enter the entangled regime and therefore quickly become too viscous to be extruded at a rapid rate, instead approaching bead-on-string morphologies as the surface evaporation outpaces the extrusion. Conversely, when the loading is low, the gel will be weak enough to allow for the emission of child droplets during the extrusion. The competition between viscous relaxation time and evaporation time results in the peak in AR seen in Fig. 3 at 0.5 wt%. It is important to contrast the difference between NWs formed in this range of loadings and the tailed and elongated particles reported previously by Almería et al.[16] Indeed, all concentrations we tried result in the formation of NWs despite being much lower than the concentrations necessary for chain entanglement, indicating that the gelation mechanism is robust.

Molecular weight of MC has not been demonstrated to have a specific effect on the LCST temperature,[37, 48] however, the viscosity of gels, and polymer solutions in general, is linked to MW, with higher MW polymers leading to more viscous gels.[37] The effects of MW on the produced NWs is more subtle than that of the solid content within the range of MW studied, but an increase in the wire diameter can be seen in Fig. 3 for all of the higher MW MCs examined, resulting in a drop in AR for all MWs higher than the lowest of 14 kDa. Notably, there is no statistically significant change in the wire length. These results together suggest increased free volume in the final structure of the glassy NW.

Spray distance experiments were conducted at constant effective field by modulating the voltage proportionally to the distance. The effects of the spray distance are to (1) change the density of arriving NWs by expanding the spray spot and (2) to change the evaporation kinetics of the droplets, which accelerates as the heated surface is approached. This can be seen in the wire density in Fig. S8 and aspect ratios in Fig. 3, where the longer spray distance leads to longer, thinner wires. This trend explains why Zhao et al's nanopillars began to emerge at their longest spray distance (2.3 cm),[29] where the time before reaching the heated substrate was sufficient to allow the crystalizing polymer solution to pass through a gel-like state.

We employed four different additives expected to have contrasting effects: (1) silica nanoparticles, (2) ethylene glycol (EG), (3) polyethylene glycol (PEG), and (4) poly(vinylpyrrolidone)-capped gold nanoparticles (discussed in the next section). All additives were substitutional, meaning that the total solids content in the drop was fixed. Silica nanoparticles can be expected to increase uniformly the

viscosity of the droplet as the solvent evaporates independent of the gelation, leading eventually to complete jamming. As a result, nanowire formation is halted mid-generation as a elongated bead-on-string morphology (Fig. 4a, with the full series shown in Fig. S10). In contrast, ethylene glycol can be viewed as a plasticizer, lowering the viscosity of the gel and raising the gel temperature;[43] however, it is also volatile. This means that, much as with the evaporating droplets of the usual spray case, there will be a natural viscosity gradient from the outside to the inside of the droplet, resulting in beads-on-strings despite having an overall lower mean viscosity (Fig. 4b, with the full series shown in Fig. S10). Raising the MW of the ethylene glycol by switching to low MW polyethylene glycol (400 Da) removes the volatility. At the same time, the hydrophilic PEG may enhance gelation through depletion. The net result creates longer, thinner wires at the same loading that previously resulted in bead-on-string morphologies, providing evidence that the presence of any viscosity gradient will prevent the NW formation (Fig. 4c, with the full series shown in Fig. S11). This was verified with single wire measurements shown in Fig. 3; however, the apparent effect in the single wire was smaller than the effect observed in the lattice qualitatively. This suggests that the presence of the non-volatile plasticizer allows for additional extrusion of the NWs created by the presence of the building electric field in the NW foam. Equivalently, the foam expands to lower the overall charge density and counter field developing on the target.

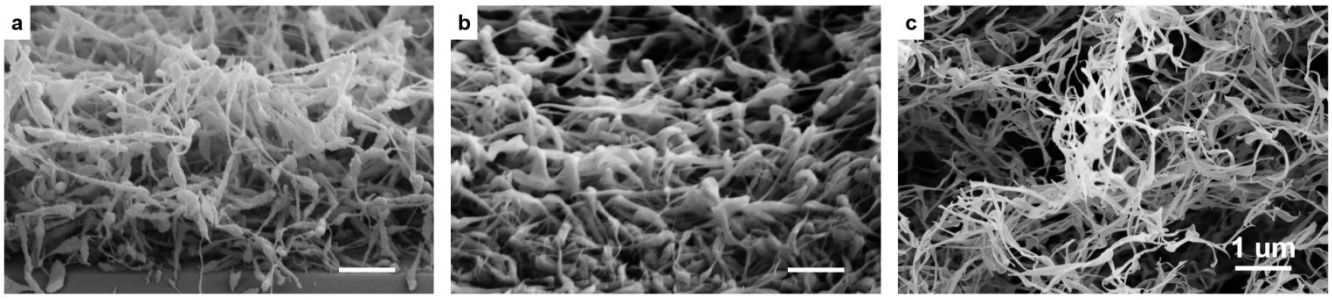


**Fig. 4** SEM images of 14 kDa MC sprayed with different additives as 1 wt % from a 3:2 weight-basis water:ethanol blend in different mass ratios. (a) MC:silica particles (1:5) sprayed for 60 min; (b) MC:EG (5:1) sprayed for 60 min; (c) MC:PEG 400 (5:1) sprayed for 30 min. All sprays were conducted at a flow rate of 0.25 mL/hr, a spray distance of 4 cm, and with a substrate temperature of 90 °C.

Application to Functional CoatingsThe ability to obtain a wide variety nanowire forests using low temperature, ambient condition spray processing at a highly scalable rate could be a huge benefit for continuous processes such as roll-to-roll manufacturing. In addition, these MC wires have the necessary properties to be a self-limiting electrospray deposition (SLED) as defined in our recent manuscript[49] and confirmed by a hole depth array approach we have recently demonstrated (Fig. S13).[50] SLED enables the coating of complex 3D objects. As there are many methods for conversion structures of polymeric materials into other materials, by coating, pyrolysis, and sol gel methods, this work can be viewed as a starting point for the fabrication of a host of 1D architectures. Additionally, the MC NWs can "host" other materials, as shown with the gold nanoparticle results in Fig. 5a, b. The goal of these experiments was, instead of to manipulate the viscosity of the forming wire, to demonstrate the ability to enhance the functionality of the deposit materials using these manipulations. In this case, the NW morphology prevents particle agglomeration and the resultant broadening of the single-particle plasmon as shown in spectroscopic reflectometer experiments. It can be seen that two plasmon peaks emerge, characteristic of single particles (~545 nm) and close-packed 1D particle chains (~650 nm).[51, 52] The relative intensity of the single-particle peak increases faster for the PEG sample, indicating the effect of the modifier in producing longer wires. This demonstrates the ability to isolate the single-particle behaviour within the composite. Through this mechanism, high surface area 3D foams of optically active foams can be applied hierarchically to complex 3D surfaces (Fig. 5c and Supplementary Movie 4).

## Conclusion

We have shown that homogenous viscosity transitions lead to the formation of NW forests and foams by electrospinning on an individual droplet level. Specifically, we employed the gelation of cellulose ethers, likely accelerated by charge and shear mechanisms, as a means to achieve this transition. Further, we demonstrated that the NWs formed in this way could be utilized as containers to isolate plasmonic gold nanoparticles for functional coatings. This is just a single example of functional particles that could be explored. More importantly, it is critical to note that while we have only observed the formation of these wires in cellulose ethers, other viscosity transitions (*e.g.*, crystalline polymers, liquid crystals) could lead to these same NW structures, should appropriate kinetics be achievable. What is established, then, is a "recipe" for achieving the NW morphology—the abrupt increase in droplet viscosity in air. It remains to future investigation to accomplish this in other materials systems. This study additionally highlights that the formation of morphologies during ESD spray, despite being experimentally employed for several decades, is still relatively under-investigated. The interplay of extreme electrostatic forces with dynamic viscous fluidics and self-assembly can result in new and beautiful morphological evolution and create a novel manufacturing platform for functional materials and coatings.

COMMUNICATION

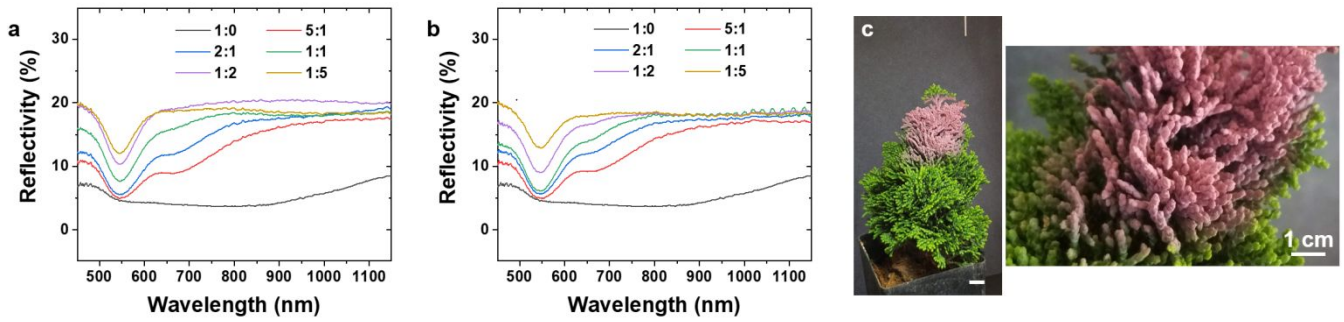


**Fig. 5** Blends of MC and gold nanoparticles. (a, b) Reflection spectra of (a) sprayed 0.3 wt% 14 kDa MC:50 nm gold nanoparticles in different mass ratios; (b) sprayed 0.3 wt% (5 14 kDa MC:1 PEG 400):50 nm gold nanoparticles in different mass ratios; All sprays were conducted at a spray distance of 4 cm with a flow rate of 0.15 mL/hr for 30 min at the substrate temperature of 90 °C in 3:2 weight-basis water:ethanol blend. (c) Photographs of a complex 3D surface coating of a Thoweil Hinoki Cypress with 0.3 wt% 5:1 (5 14 kDa MC:1 PEG 400):50 nm gold nanoparticles in 3:2 weight-basis water:ethanol blend at a minimum spray distance of ~5 cm with a flow rate of 0.2 mL/hr for 30 hr at room temperature. The zoomed in view reveals the conformal coating of the forest on the tree.

## Conflicts of interest

Authors declare no competing interests.

## Acknowledgements

J. P. S. acknowledges funding from the 3M Corporation through the 3M Non-Tenured Faculty Award. X. Y., S. C., and T. F. M. acknowledge funding through the American Chemical Society Petroleum Research Fund No. 56884-DNI9. C. J. N. acknowledges funding from the Rutgers Aresty Summer Scholars Program. X. Y. acknowledges computational resources provided by the Watson Data Center at Binghamton University and the Center for Functional Nanomaterials, which is a U.S. DOE Office of Science Facility, at Brookhaven National Laboratory under Contract No. DESC0012704. The authors thank Prof. Timothy Lodge for useful discussion.

## Notes and references

1. L. Persano, A. Camposeo, C. Tekmen and D. Pisignano, *Macromolecular Materials and Engineering*, 2013, **298**, 504-520.
2. L. N. Blumberg, J. C. Gursky and P. C. Stein, *Electrospraying of Thin Targets*, Los Alamos Scientific Laboratory, 1962.
3. M. Yamashita and J. B. Fenn, *The Journal of Physical Chemistry*, 1984, **88**, 4451-4459.
4. A. Jaworek and A. T. Sobczyk, *J. Electrostatics*, 2008, **66**, 197-219.
5. S. Kavadiya and P. Biswas, *J. Aerosol Sci*, 2018, DOI: https://doi.org/10.1016/j.jaerosci.2018.04.009.
6. K. Morota, H. Matsumoto, T. Mizukoshi, Y. Konosu, M. Minagawa, A. Tanioka, Y. Yamagata and K. Inoue, *Journal of colloid and interface science*, 2004, **279**, 484-492.
7. T. Mizukoshi, H. Matsumoto, M. Minagawa and A. Tanioka, *Journal of applied polymer science*, 2007, **103**, 3811-3817.
8. M. Nasir, H. Matsumoto, M. Minagawa, A. Tanioka, T. Danno and H. Horibe, *Polymer journal*, 2009, **41**, 402-406.
9. B. Almería and A. Gomez, *Journal of colloid and interface science*, 2014, **417**, 121-130.
10. K. Altmann, R.-D. Schulze and J. Friedrich, *Thin solid films*, 2014, **564**, 269-276.
11. I. B. Rietveld, K. Kobayashi, H. Yamada and K. Matsushige, *Journal of colloid and interface science*, 2006, **298**, 639-651.
12. K. Kawakami, *International journal of pharmaceutics*, 2012, **433**, 71-78.
13. I. B. Rietveld, K. Kobayashi, H. Yamada and K. Matsushige, *Soft Matter*, 2009, **5**, 593-598.
14. A. Rezvanpour and C.-H. Wang, *Chemical engineering science*, 2011, **66**, 3836-3849.
15. S. Hao, Y. Wang, B. Wang, J. Deng, L. Zhu and Y. Cao, *Materials Science and Engineering: C*, 2014, **39**, 113-119.
16. B. Almería, W. Deng, T. M. Fahmy and A. Gomez, *J. Colloid Interface Sci.*, 2010, **343**, 125-133.
17. J. Xie, J. C. Tan and C.-H. Wang, *Journal of pharmaceutical sciences*, 2008, **97**, 3109-3122.
18. G. H. McKinley, *Bulletin of the Society of Rheology*, 2005, 6-9.
19. P. G. Lepe, N. Tucker, A. J. Watson, D. LeCorre-Bordes, A. J. Fairbanks and M. P. Staiger, *Applied Rheology*, 2017, **27**, 18-27.
20. J. F. Hoburg, *ITIA*, 1982, 666-672.
21. Y. Han and J. Dong, *Journal of Micro and Nano-Manufacturing*, 2018, **6**.

22. H. You, Y. Yang, X. Li, K. Zhang, X. Wang, M. Zhu and B. S. Hsiao, *Journal of Membrane Science*, 2012, **394-395**, 241-247.
23. L. Zhao, C. Song, M. Zhang and Y. Zheng, *Chem. Commun.*, 2014, **50**, 10651-10654.
24. M. Al-Qadhi, N. Merah, A. Matin, N. Abu-Dheir, M. Khaled and K. Youcef-Toumi, *Journal of Polymer Research*, 2015, **22**, 1-9.
25. A. Gomez and K. Tang, *Physics of Fluids*, 1994, **6**, 404-414.
26. R. T. Collins, K. Sambath, M. T. Harris and O. A. Basaran, *Proceedings of the National Academy of Sciences*, 2013, **110**, 4905-4910.
27. D. Duft, T. Achtzehn, R. Müller, B. A. Huber and T. Leisner, *Nature*, 2003, **421**, 128-128.
28. M. H. Merrill, I. I. I. W. R. Pogue and J. N. Baucom, *Journal of Micro and Nano-Manufacturing*, 2015, **3**, 011003-011003.
29. X.-Y. Zhao, D. E. Johnston, J. C. Rodriguez, Z. Tao, B.-X. Mi and W. Deng, *Macromolecular Materials and Engineering*, 2017, **302**, 1700090.
30. R. D. Groot and P. B. Warren, *The Journal of Chemical Physics*, 1997, **107**, 4423-4435.
31. P. Español and P. B. Warren, *The Journal of Chemical Physics*, 2017, **146**, 150901.
32. P. Español, *Physical Review E*, 1995, **52**, 1734-1742.
33. R. D. Groot, *The Journal of Chemical Physics*, 2003, **118**, 11265-11277.
34. S. Qin and X. Yong, *Soft Matter*, 2017, **13**, 5137-5149.
35. S. Qin, J. Kang and X. Yong, *Langmuir*, 2018, **34**, 5581-5591.
36. W. A. Sirignano, *Fluid dynamics and transport of droplets and sprays*, Cambridge university press, 2010.
37. J. W. McAllister, P. W. Schmidt, K. D. Dorfman, T. P. Lodge and F. S. Bates, *Macromolecules*, 2015, **48**, 7205-7215.
38. S. Morozova, *Polym. Int.*, 2020, DOI: 10.1002/pi.5945.
39. J. R. Lott, J. W. McAllister, M. Wasbrough, R. L. Sammler, F. S. Bates and T. P. Lodge, *Macromolecules*, 2013, **46**, 9760-9771.
40. J. W. McAllister, J. R. Lott, P. W. Schmidt, R. L. Sammler, F. S. Bates and T. P. Lodge, *ACS Macro Letters*, 2015, **4**, 538-542.
41. S. Morozova, P. W. Schmidt, A. Metaxas, F. S. Bates, T. P. Lodge and C. S. Dutcher, *ACS Macro Letters*, 2018, **7**, 347-352.
42. H. Takeshita, K. Saito, M. Miya, K. Takenaka and T. Shiomi, *Journal of Polymer Science Part B: Polymer Physics*, 2010, **48**, 168-174.
43. G. Levy and T. W. Schwarz, *Journal of the American Pharmaceutical Association*, 1958, **47**, 44-46.
44. Y. Xu, L. Li, P. Zheng, Y. C. Lam and X. Hu, *Langmuir*, 2004, **20**, 6134-6138.
45. M. B. Salehi, M. V. Sefti, A. M. Moghadam and A. D. Koohi, *Journal of Macromolecular Science, Part B*, 2012, **51**, 438-451.
46. A. Frenot, M. W. Henriksson and P. Walkenström, *J. Appl. Polym. Sci.*, 2007, **103**, 1473-1482.
47. A. M. Gañán-Calvo, J. Dávila and A. Barrero, *J. Aerosol Sci*, 1997, **28**, 249-275.
48. P. L. Nasatto, F. Pignon, J. L. Silveira, M. E. R. Duarte, M. D. Noseda and M. Rinaudo, *Polymers*, 2015, **7**, 777-803.
49. L. Lei, D. A. Kovacevich, M. P. Nitzsche, J. Ryu, K. Al-Marzoki, G. Rodriguez, L. C. Klein, A. Jitianu and J. P. Singer, *ACS Applied Materials & Interfaces*, 2018, **10**, 11175-11188.
50. D. A. Kovacevich, L. Lei, D. Han, C. Kuznetsova, S. E. Kooi, H. Lee and J. P. Singer, *ACS Applied Materials & Interfaces*, 2020, **12**, 20901-20911.
51. Q. H. Wei, K. H. Su, S. Durant and X. Zhang, *Nano Letters*, 2004, **4**, 1067-1071.
52. K. H. Su, Q. H. Wei, X. Zhang, J. J. Mock, D. R. Smith and S. Schultz, *Nano Letters*, 2003, **3**, 1087-1090.

We demonstrate that homogeneous gelation of droplets in electrospray leads to the generation of nanowire forests and foams.